Absorption and scattering properties of dense ensembles of nonspherical particles

Jean-Claude Auger,[1] Vincent Martinez,[2] and Brian Stout[3,*]

[1]*Center for Laser Diagnostics, Department of Applied Physics, Yale University, New Haven, Connecticut 06520 USA*
[2]*Department of Applied Physics, RMIT University, Melbourne, Victoria 3000, Australia*
[3]*Institut Fresnel D.U. St Jérôme UMR 6133, 13397 Marseille Cedex 20, France*
[*]*Corresponding author: brian.stout@fresnel.fr*

Received May 3, 2007; revised July 17, 2007; accepted July 19, 2007;
posted September 10, 2007 (Doc. ID 82731); published October 17, 2007

The purpose of this work is to show that an appropriate multiple T-matrix formalism can be useful in performing qualitative studies of the optical properties of colloidal systems composed of nonspherical objects (despite limitations concerning nonspherical particle packing densities). In this work we have calculated the configuration averages of scattering and absorption cross sections of different clusters of dielectric particles. These clusters are characterized by their refraction index, particle shape, and filling fraction. Computations were performed with the recursive centered T-matrix algorithm (RCTMA), a previously established method for solving the multiple scattering equation of light from finite clusters of isotropic dielectric objects. Comparison of the average optical cross sections between the different systems highlights variations in the scattering and absorption properties due to the electromagnetic interactions, and we demonstrate that the magnitudes of these quantities are clearly modulated by the shape of the primary particles. © 2007 Optical Society of America

OCIS codes: 290.4020, 290.4210, 290.5850.

1. INTRODUCTION

Due to the wide range of possible applications in industrial and academic research, accurate and fast numerical formalisms for calculating the scattering and absorption properties of light by nonspherical dielectric objects are of considerable interest. Several theoretical approaches have successfully been employed in different fields of applications. Among them, let us mention the discrete dipole approximation [1], the finite-difference time-domain Method (FDTDM) [2], and the single T-matrix formalism [3].

The latter formalism, originally developed by Waterman and largely extended by Mishchenko [4], has proven to be quite efficient for a number of reasons: it permits accurate and relatively fast calculations of the optical properties of axisymmetrical isotropic metallic or dielectric objects, and it also permits explicit analytical evaluations of orientation averages of various cross sections and of the scattering matrix elements of ensembles of independent scatterers, consequently avoiding time consuming numerical integrations over a large series of Euler's angles. Furthermore, the symmetries in particle shape can be exploited to increase the stability and speed of the numerical evaluation of the T-matrix coefficients [5].

Despite the above-mentioned benefits, the null-field T-matrix formalism suffers from several non-negligible disadvantages. Among these, we should mention the numerical instability of T-matrix computations for sufficiently elongated or flattened objects. Another difficulty is the improper exploitation of the surface integral equation (as discussed in [6]) to numerically evaluate T matrices of nonaxisymmetric particles. Finally, we mention the general T-matrix inconvenience of imposing circumscribing spheres around nonspherical scatterers in order to expand the electric and magnetic fields in terms of spherical wave basis sets.

A variety of studies have proposed ways of alleviating the first two of the aforementioned restrictions and improve the initial T-matrix formalism. Among the many we can cite are the improvement of T-matrix computations to nonabsorbing and weakly absorbing particles having large aspect ratios [7], the extension of the null-field method to evaluate the optical properties realistically shaped particles [8], and the computation of T-matrix coefficients in spheroidal coordinate systems [9].

A great strength of T-matrix formalism is that it readily allows multiple-scattering calculations of the optical properties of ensembles of isotropic dielectric spheres [10]. This technique has proven useful in colloidal science by modeling arbitrarily shaped objects as agglomerations of spherical particles. In principal then, the multiple spheres T-matrix approach is applicable in calculating the optical properties of collections of coupled nonspherical objects. Nevertheless, the multiple-scattering method does not directly allow a treatment of close-packed clusters of nonspherical particles commonly encountered in spores or other types of biological and inorganic substances. Consequently, many studies of such aggregates in applied research are performed with alternative techniques [11].

The purpose of this work is to show that in spite of the disadvantage linked to the prohibition of close-packing configurations, the multiple T-matrix formalism can be a relevant tool to study the optical properties of real colloi-

dal systems composed of nonspherical particles. Applications can be found in the paint industry where it is well known from empirical observations that color and opacity of colloids can be modified by slight variations in shape, orientation, or concentrations of the scattering particles in the dispersed phase.

In practice, all the studies performed to model the optical properties of paint films are based on the radiative transfer equation and the assumption of independent scattering processes to calculate the local properties of the medium. In addition, although there are rare exceptions [12], the scattering particles are usually supposed to be spherical, neglecting other possible shapes.

In this work, we show that the multiple T-matrix formalism can, when combined with an adequate statistical approach, be applied to calculate the averaged optical properties of different types of particle clusters, with these clusters representing mesoscopic volumes of a colloidal system. These clusters types in turn are characterized by the size and shape of their primary particles. Qualitative comparisons between the scattering and absorption cross sections of the different systems can be used as a guide in understanding the variations in reflection or transmission coefficients of the real colloidal media as function of the morphological characterization of their dispersed phases. In such studies, effects of electromagnetic couplings can be quantified and analyzed by changing the apparent filling fraction of the ensemble of particles.

This article is structured as follows. In the first section we briefly recall the fundamental aspects of the multiple-scattering T-matrix formalism, emphasizing its extension to nonspherical objects. In the second section, we present the method that we used to generate the different configuration of collections of particles. We also clarify the statistical process used to evaluate the configuration averaged cross sections and their standard deviations. The third section is dedicated to the study of an example of a possible application.

2. THEORY

A. Multiple T Matrix: General Formalism

We consider a monochromatic plane wave with amplitude E_0 and wavelength λ_0 impinging on an ensemble of N arbitrarily oriented dielectric objects randomly dispersed in an infinite nonabsorbing medium. The center of each particle is defined in a principal coordinate system $\Re_0$ by a position vector $\mathbf{x}^{(i)}$ (i being the particle label). The complex indices of refraction of the individual particles are denoted $n_p^{(i)}$, while n_0 denotes the index of the host medium. The wave vector of the incident field is noted $\mathbf{k}_{inc}$ with $k \equiv \|\mathbf{k}\| = 2\pi n_0/\lambda_0$. In the multiple-scattering T-matrix formalism, the incident and scattered electric fields are expanded in terms of an infinite series of spherical vector wave functions $\{\mathbf{\Psi}_{1nm}(k\mathbf{r}), \mathbf{\Psi}_{2nm}(k\mathbf{r})\}$ ($\mathbf{\Psi}_{1nm}(k\mathbf{r})$ and $\mathbf{\Psi}_{2nm}(k\mathbf{r})$ historically being denoted respectively as $\mathbf{M}_{nm}(k\mathbf{r})$ and $\mathbf{N}_{nm}(k\mathbf{r})$). Following the commonly employed condensed matrix notation [13], the incident field $\mathbf{E}_{inc}$ and the fields scattered respectively by the individual scatterers, $\mathbf{E}_{sca}^{(i)}$ ($i=1,\ldots,N$), can be expressed in terms of their coefficients on the spherical wave basis:

$$\begin{aligned}\mathbf{E}_{inc} &= E_0 \sum_{n=1}^{\infty} \sum_{m=-n}^{n} [Rg\{\Psi_{1nm}^t(k\mathbf{r})\}a_{1nm} + Rg\{\Psi_{2nm}^t(k\mathbf{r})\}a_{2nm}] \\ &\equiv E_0 Rg\{\Psi^t(k\mathbf{r})\}a, \\ \mathbf{E}_{sca}^{(i)} &= E_0 \sum_{n=1}^{\infty} \sum_{m=-n}^{n} [\Psi_{1nm}^t(k\mathbf{r}_i)f_{1nm}^{(i)} + \Psi_{2nm}^t(k\mathbf{r}_i)f_{2nm}^{(i)}] \\ &\equiv E_0 \Psi^t(k\mathbf{r}_i)f^{(i)}, \end{aligned} \tag{1}$$

where $\mathbf{r}_i \equiv \mathbf{r} - \mathbf{x}_i$ and $Rg\{\}$ and t stand respectively for "regular part of" and "transpose." The column "vector" of the expansion coefficients of the incident field $\mathbf{E}_{inc}$ is denoted a, whereas the column vectors containing the scattering coefficients of the individual scatterers are denoted $f^{(i)}$. We remark in Eq. (1) that the incident field is written in terms of spherical coordinates centered on $\Re_0$, whereas the scattered fields are expressed in spherical coordinate systems centered on $\Re_i$ (i.e., the center of the ith object located at $\mathbf{x}^{(i)}$). Following the standard Foldy–Lax formulation, the total excitation electric field on the ith particle of the system is expressed: $\mathbf{E}_{exc}^{(i)} = \mathbf{E}_{inc} + \sum_{\substack{j=1 \\ j\neq i}}^{N} \mathbf{E}_{sca}^{(j)}$. The spherical wave expressions of the excitation fields for the individual particles is [14,15]

$$\mathbf{E}_{exc}^{(i)} = Rg\{\Psi^t(k\mathbf{r}_i)\}\left[J^{(i,0)}a + \sum_{\substack{j=1 \\ j\neq i}}^{j=N} H^{(i,j)}f^{(j)}\right] \equiv Rg\{\Psi^t(k\mathbf{r}_i)\}e^{(i)}, \tag{2}$$

where $e^{(i)}$ are the coefficients of the excitation field of the ith particle, while $J^{(i,0)}$ and $H^{(i,j)}$ represent matrices that translate the spherical wave functions from one reference frame to another [14,15]. Now, combining Eq. (2) with the definition of the single particle T-matrices, namely $f^{(i)} \equiv T_1^{(i)}e^{(i)}$, leads to a series of N-coupled equations with unknown scattering coefficient vectors $f^{(i)}$:

$$f^{(i)} = T_1^{(i)}\left[J^{(i,0)}a + \sum_{\substack{j=1 \\ j\neq i}}^{j=N} H^{(i,j)}f^{(j)}\right], \qquad i = 1,\ldots,N. \tag{3}$$

These relations have the inconvenience that they depend on the incident field coefficients, a. It is then advantageous to introduce $T_N^{(i)}$, as the N-particle T-matrix of the ith object, which is defined (see below) so as to include all the information about the multiple-scattering effects caused by the presence of the other objects. Its formulation directly links the scattered field to the incident field via the relation $f^{(i)} = T_N^{(i)}J^{(i,0)}a$. Inserting this definition into Eq. (3) leads to a new linear system of coupled equations whose unknowns are now the N-scatterer T matrices:

$$T_N^{(i)} = T_1^{(i)}\left[\overleftrightarrow{\mathbf{I}} + \sum_{\substack{j=1 \\ j\neq i}}^{N} H^{(i,j)}T_N^{(j)}J^{(j,i)}\right], \qquad i = 1,\ldots,N. \tag{4}$$

Different formalisms based on iterative and recursive processes have been successfully developed to solve Eq. (4) [16–19]. Once the N-scatterer T matrices have been deter-

mined, the total cross sections of the N interacting particles can be easily calculated [20,21]. Finally, let us recall that in practice, the computation of the $T_1^{(i)}$ matrices requires the truncation of an infinite-dimensional integral matrix equation to a value $n=n_{max}$. This value must be large enough to represent the physically relevant partial waves impinging on the object correctly but not too large to be useful numerically. It is usually admitted that n_{max} must be at least proportional to the particle's size parameter to reach a good precision in the calculation. Looking back at Eq. (1), we see that for a $n=n_{max}$ truncation, the total number of each type of spherical waves in the field expansion is $2n_{max}(n_{max}+2)$. Consequently, the dimension of each matrix in Eq. (4) is $(2n_{max}(n_{max}+2))^2$.

B. Application to Nonspherical Objects

Multiple T-matrix formalism can be successfully extended to nonspherical objects providing that the following three conditions are fulfilled:

- C_1: the relative positions between the particles' centers must be such that the smallest circumscribing spheres (CSs) surrounding each object do not overlap.
- C_2: every single T-matrix $T_1^{(i)}$ must be numerically stable, well conditioned, and judiciously truncated.
- C_3: the linear system given by Eq. (4) must be solvable to a good precision in a reasonable lapse of computer time.

The first requirement is linked to a theoretical constraint imposed by the extended boundary condition technique and the use of the homogeneous spherical waves as the common basis to expand the electromagnetic fields. Its first consequence is to limit the number of possible spatial arrangements. In particular, it forbids the study of compact clusters composed by nonspherical objects (see Fig. 1). The second consequence is a strong dependence of the maximal volumetric concentration of the system on the aspect ratios of the constituent particles. As shown in Fig. 2, at constant volume, the more elongated or flattened the constituent objects, the lower the maximum number of particles by unit volume that can be treated. Since low filling fractions are obviously less convenient for studying electromagnetic couplings between particles, a compromise must be reached between the value of the aspect ratio and the maximum filling fraction to be analyzed.

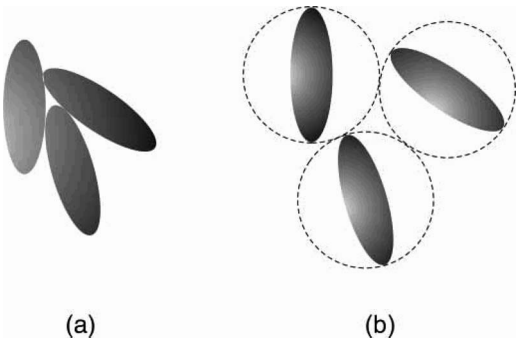

Fig. 1. Spatial arrangements of aggregated nonspherical particles (a) without circumscribing sphere spatial constraints and (b) with circumscribing sphere spatial constraints.

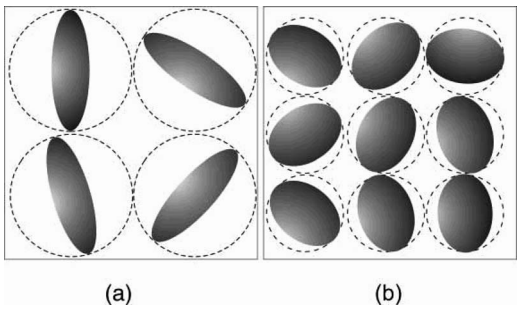

Fig. 2. Relations between the aspect ratio of the nonspherical particles and the maximum filling fraction obtainable for the system under the hypothesis of the smallest circumscribing spheres restriction (a) large aspect ratio (b) small aspect ratio.

Condition C_2 restricts the particles' intrinsic properties such as their complex indexes of refraction, their shape, and their dimensions. Indeed, the calculation of the T matrix coefficients is performed in two steps: the resolution of two truncated infinite-dimensional integral matrix equations involving the electromagnetic fields on the particles' surface and a matrix inversion. The later operation cannot be accurately performed if the original matrix is not well conditioned or if it is close to a singularity. Such conditions generally arise for highly rough or sharp surfaces, strongly scattering or absorbing objects, as well as those with disproportionate aspect ratios.

Condition C_3 controls the total number of particles because the dimension of the linear system given by Eq. (4) varies as function of N and $(n_{max})^2$. Systems composed of many objects with a relatively small-size parameter can be treated quite easily, while only a few objects characterized by large-size parameters can be handled in a reasonable lapse of time.

Finally, since conditions C_2 and C_3 partially depend on the computer power and the type of algorithms used to perform the study, they can be improved upon to a certain degree. However, the condition C_1 is imposed by theoretical constraints and consequently seems to be unavoidable within the current framework.

3. METHODOLOGY

A. Cell Builder

We consider N_s particles having volume $v_p^{(i)}$ and complex index of refraction $\tilde{n}_p^{(i)}$ $(i=1,\ldots,N_s)$ embedded in a finite nonabsorbing medium with index of refraction n_0. The filling fraction of the total system is given by f_p such that particles can be dispersed only into a spherical volume V_0, centered at the origin of the main reference frame $\mathfrak{R}_0$. We note by $R_p^{(i)}$, the radius of the CS corresponding to the ith object. The application of multiple T-matrix algorithm of the previous section implicitly requires the knowledge of the particles' orientation and position $\mathbf{x}^{(i)}$. The above parameters are invoked in the following procedure:

- V_0 with radius R_0 is evaluated from the knowledge of N, f_p, and $v_p^{(i)}$.
- The Cartesian coordinates, $x^{(i)}$, $y^{(i)}$, $z^{(i)}$ of the position vectors $\mathbf{x}^{(i)}$ are selected from a uniform random process subject to the constraints $\|\mathbf{x}^{(i)}\| \leq (R_0 - R_p^{(i)})$ and $\|\mathbf{x}^{(i)} - \mathbf{x}^{(j)}\|$

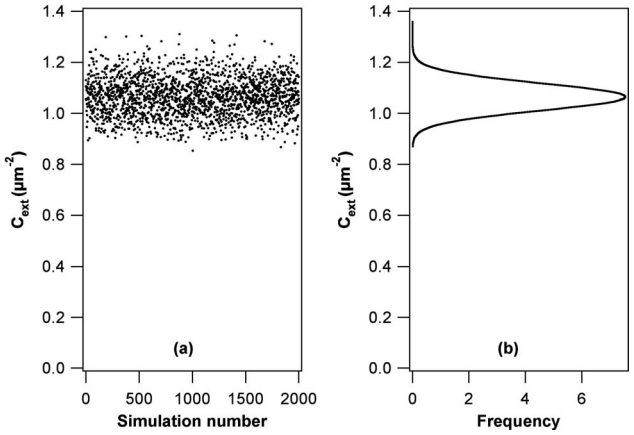

Fig. 3. Statistical treatment. (a) Representation of the extinction cross sections as function of the different random configurations of the system. (b) Gaussian adjustment from the previous set of data describing the probability for the system to possess a given value of the extinction cross section.

$\geqslant (R_p^{(i)}+R_p^{(j)})$ for $i \neq j$. The first of these constraints ensures that the particles are entirely localized within V_0, while the latter guarantees the satisfaction of condition C_1.

- The particles' orientation defined with respect to $\Re_i$ are generated by a uniform random process on the Euler angles $(\alpha^{(i)}, \beta^{(i)}, \gamma^{(i)})$.

The latter procedure can be applied in cycles in order to determine N_c different configurations involving the same particles and separations.

B. Statistical Treatment

Once that N_c cluster configurations have been generated, the recursive centered T-matrix algorithm (RCTMA) [19] is used to calculate the extinction (C_{ext}), scattering (C_{sca}), and absorption (C_{abs}) cross sections corresponding to both the TE and TM polarizations of the incident fields while keeping $\hat{\mathbf{k}}_{inc}$ parallel to the Oz axis of the principal reference frame. The N_c resulting cross sections are fitted with a Gaussian distribution function characterized by an average value and a standard deviation noted respectively $\langle C_j \rangle$ and σ_j [see Figs. 3(a) and 3(b)] where j stands for *ext*, *sca*, or *abs*. The term "frequency" used in our figures corresponds to the probability of finding an extinction cross section with value C_j after averaging over N_c random configurations.

4. APPLICATION

We have compared the absorption and scattering cross sections of three different systems noted S_1, S_2, and S_3 composed of $N_s=6$ particles. Each system was composed of three respective types of primary particles all having identical volumes: (S_1) oblate spheroids with axes measuring 0.078 and 0.157 μm, (S_2) prolate spheroids with axes of 0.198 and 0.099 μm, and (S_3) spheres with radii of 0.125 μm. For simplicity we chose the vacuum ($n_0=1$) as the surrounding medium and the wavelength of the incident field was fixed as 0.545 μm, corresponding to the

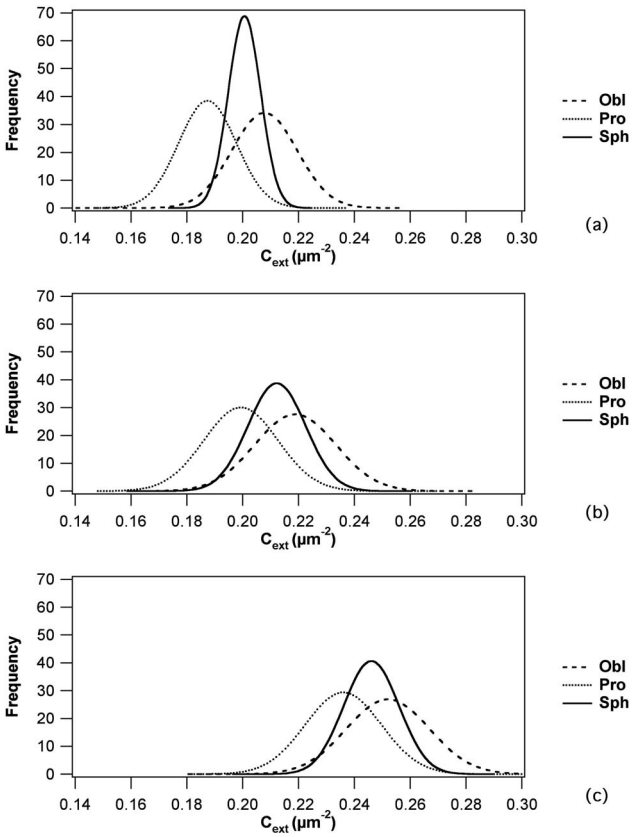

Fig. 4. Frequency as a function of the extinction cross sections for the spherical, oblate, and prolate systems with index of refraction $n_p=1.5$: (a) $f_p=0.002$, (b) $f_p=0.03$, (c) $f_p=0.07$.

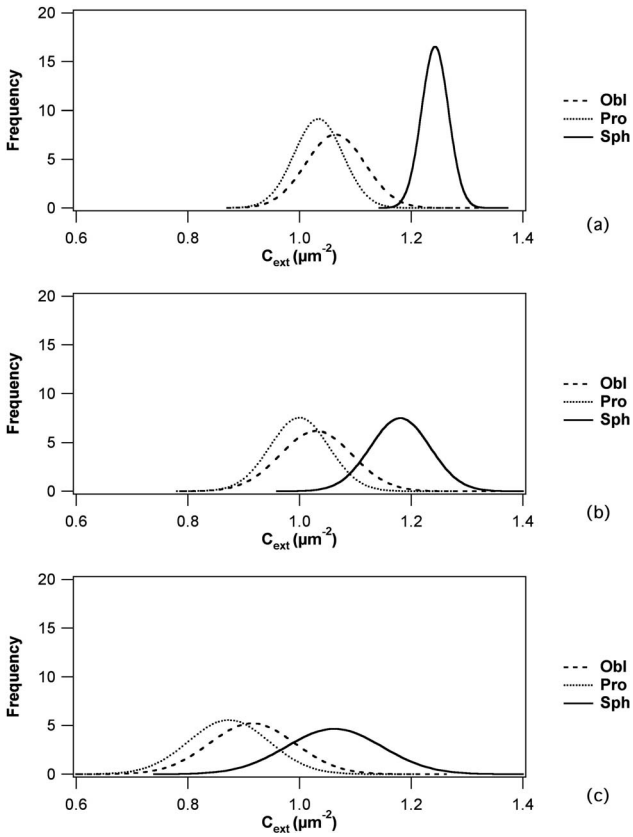

Fig. 5. Frequency as function of the extinction cross sections for the spherical, oblate, and prolate systems with index of refraction $n_p=2.8$: (a) $f_p=0.002$, (b) $f_p=0.03$, (c) $f_p=0.07$.

Table 1. Values of the Average Extinction Cross Sections and Standard Deviations Obtained from Fig. 4 and Related to the Systems Having $n_p=1.5$

	$\langle C_{ext}\rangle$			σ		
$n_p=1.5$	S_1	S_2	S_3	S_1	S_2	S_3
$f_p=0.002$	0.208	0.187	0.201	0.016	0.015	0.008
$f_p=0.030$	0.219	0.199	0.212	0.020	0.019	0.015
$f_p=0.070$	0.252	0.236	0.246	0.021	0.019	0.015

Table 2. Values of the Average Extinction Cross Sections and Standard Deviations Obtained from Fig. 5 and Related to the Systems Having $n_p=2.8$

	$\langle C_{ext}\rangle$			σ		
$n_p=2.8$	S_1	S_2	S_3	S_1	S_2	S_3
$f_p=0.002$	1.064	1.034	1.243	0.075	0.062	0.034
$f_p=0.030$	1.030	1.000	1.180	0.091	0.075	0.075
$f_p=0.070$	0.915	0.873	1.062	0.108	0.102	0.122

Table 3. Values of the Average Absorption Cross Sections and Standard Deviation Obtained from Fig. 6 and Related to the Systems Having $n_p=1.5+i1.0$

	$\langle C_{abs}\rangle$			σ		
$n_p=1.5+i1.0$	S_1	S_2	S_3	S_1	S_2	S_3
$f_p=0.002$	0.487	0.515	0.4798	0.0146	0.0184	0.0111
$f_p=0.030$	0.470	0.495	0.462	0.0253	0.0275	0.0237
$f_p=0.070$	0.410	0.429	0.406	0.0201	0.0208	0.0186

Table 4. Values of the Average Scattering Cross Sections and Standard Deviation Obtained from Fig. 7 and Related to the Systems Having $n_p=1.5+i1.0$

	$\langle C_{sca}\rangle$			σ		
$n_p=1.5+i1.0$	S_1	S_2	S_3	S_1	S_2	S_3
$f_p=0.002$	0.297	0.275	0.291	0.0157	0.0109	0.0028
$f_p=0.030$	0.294	0.273	0.288	0.0149	0.0109	0.0048
$f_p=0.070$	0.282	0.269	0.278	0.0135	0.0104	0.0078

Table 5. Values of the Average Absorption Cross Sections and Standard Deviation Obtained from Fig. 8 and Related to the Systems Having $n_p=2.8+i1.0$

	$\langle C_{abs}\rangle$			σ		
$n_p=2.8+i1.0$	S_1	S_2	S_3	S_1	S_2	S_3
$f_p=0.002$	0.505	0.516	0.469	0.0156	0.0184	0.0120
$f_p=0.030$	0.486	0.496	0.453	0.0315	0.0297	0.0260
$f_p=0.070$	0.420	0.427	0.397	0.0216	0.0214	0.0195

Table 6. Values of the Average Scattering Cross Sections and Standard Deviation Obtained from Fig. 9 and Related to the Systems Having $n_p=2.8+i1.0$

	$\langle C_{sca}\rangle$			σ		
$n_p=2.8+i1.0$	S_1	S_2	S_3	S_1	S_2	S_3
$f_p=0.002$	0.532	0.439	0.443	0.0464	0.0464	0.0046
$f_p=0.030$	0.515	0.428	0.431	0.0443	0.0441	0.0097
$f_p=0.070$	0.464	0.397	0.398	0.0383	0.0385	0.021

middle of the visible spectrum. A preliminary study, dedicated to evaluating the convergence rate of $\langle C_{ext} \rangle$ and σ as function of the number of random configurations, showed that variation on $\langle C_{ext} \rangle$ and σ was on the order of 1% when going from $N_c = 1000$ to $N_c = 3000$ configurations. We therefore concluded that $N_c = 1000$ could be reliably employed in our statistic analysis in this study.

A. Nonabsorbing Particles

Figures 4 and 5 represent the Gaussian adjustments of the extinction cross sections, corresponding to S_1, S_2, and S_3 at three different concentrations: $f_p = 0.002$, 0.03, and 0.07 for $n_p = 1.5$ and $n_p = 2.8$, respectively.

1. Effect of the Concentration

Inspection of Figs. 4 and 5 clearly shows that an increase of the filling fraction from f_1 to f_3 has the same general consequences on the optical properties of all three systems, namely, a progressive shift of $\langle C_{ext} \rangle$ and a widening of the Gaussian fitted σ. The corresponding numerical values are given in Tables 1 and 2 for more details. Such variations can be explained from basic theoretical considerations.

In highly dilute systems ($f_p \ll 1$), the particles are generally far away from one another so that single scattering dominates. The weakness of electromagnetic couplings implies that the total scattering cross section of the whole system is little influenced by the relative positions of the particles. Consequently, the standard deviation is narrow and the average cross sections are close to that calculated in the independent scattering approximation. When the concentration is increased, the average distance between particles decreases, and the different orders of multiple-scattering interaction can no longer be neglected. Consequently, due to the presence of electromagnetic couplings, $\langle C_{ext} \rangle$ is shifted from its value calculated with the independent scattering assumption. Also, as interactions between the scatterers become more predominant, the probability to obtain strongly different values of C_{ext} for different configurations also increases. This effect translates as a widening of the Gaussian adjustments from Figs. 4(a)–4(c) and 5(a)–5(c). Also, because dependent scattering comes from near-field interactions between the scattered waves, the variation in the average extinction cross sections is more important when the systems evolve from $f_p = 0.03$ to $f_p = 0.07$ than from $f_p = 0.002$ to $f_p = 0.03$. At those three filling fractions, namely, $f_p = 0.002$, 0.03, and 0.07, the calculated average center-to-center distance of the particles are respectively 2.0 to 0.93 and 0.5 μm, which corresponds approximately to eight, four, and two times the diameters of their volume equivalent spheres.

2. Effect of the Index of Refraction

The value of the relative index of refraction of the system has two main effects on the optical properties of the three systems. First, it modulates the amplitude of the scattered wave intensity so that stronger scattering phenomena arise as the contrast of refraction index between the particle and surrounding medium increases. Furthermore, an increase of the scattered waves amplitudes lead to an enhancement of electromagnetic interactions between the scatterers. Inspection of Tables 1 and 2 clearly shows both effects. The average extinction cross section $\langle C_{ext} \rangle$ associated with systems having with $n_p = 1.5$ ranges from 0.187 to 0.252 μm^2, whereas it covers a range from 0.873 to 1.243 μm^2 in systems having $n_p = 2.8$. The corresponding frequencies and standard deviations are respectively lower and wider in the latter case, which translates as a higher probability of finding large differences in C_{ext} between distinct configurations.

The second effect linked to the change in the index of refraction is a difference in the sign of the relative variations of the average extinction cross sections when the filling fraction is increased. In systems with $n_p = 1.5$, electromagnetic couplings shift $\langle C_{ext} \rangle$ to higher values, while their effect is to decrease $\langle C_{ext} \rangle$ in systems with $n_p = 2.8$. If such consequences have already been observed experimentally [22] and theoretically [23], an exact modeling of the physical causes that leads to such phenomenon have not yet been proposed at our knowledge.

3. Effect of the Shape

Inspection of Figs. 4 and 5 also shows clear variations in the optical properties of the different systems as a function of the primary particles' shape. One cause of these changes is linked to the intrinsic properties of each isolated particle to scatter light. Indeed, the T-matrix coefficients are expressed as function of surface integral of different combinations of the electromagnetic fields; thus modification of the particles' shape leads to variations in the optical properties. Such phenomenon can also be explained directly from Huygens's principle, which states that the electromagnetic field in one point of space external to the scattering object can be expressed as the sum of the scattered waves originating from secondary sources located on the particles' surface. Table 7 displays the orientation and polarization average extinction cross sections for each ensemble of independent primary particles. It shows that $\langle C_{ext} \rangle$ vary from 6% to 16% when the index of refraction is 2.8, whereas they differ only slightly when it is equal to 1.5. The small differences in the latter case can be explained by the combination of three factors: a low contrast of index of refraction, relatively small values of the size parameter, and relatively modest differences in the aspect ratio of the particles. The wavelength of the incident field and the radius of the volume equivalent sphere being equal to 0.545 and 0.125 μm, respectively, the scattered field amplitude is relatively weak in this case, and the incident field cannot effectively probe the relatively light changes in the particles' shape.

Other sources of the variations in the optical properties between different systems with differing primary particles shape originates from the additional degrees of freedom that are present in configurations of ensembles of nonspherical particles. The extinction cross sections of an ensemble of nonspherical objects not only depends on the particles' relative positions (as for spherical scatterers) but also on the particles' relative orientations. Due to this supplementary degree of freedom and the presence of electromagnetic couplings, the probability of obtaining distinct extinction cross sections between two random configurations is higher in the case of systems composed of nonspherical scatterers. Consequently, the frequencies associated with spherical particles are always higher

than those of nonspherical particle systems and have a smaller dispersion coefficients, σ.

Our last remark is that the influence of the particles' shape seems to attenuate as the filling fraction increases. This attenuation is illustrated by an increasing overlapping of the Gaussian adjustments as concentration increases, even though the relative variations of the average extinction cross sections of the three systems remains relatively unchanged as the concentration varies from f_1 to f_3.

B. Absorbing Particles

Figures 6 and 7 (with Tables 3 and 4, respectively) represent the Gaussian adjustments of the scattering and absorption cross sections related to S_1, S_2, and S_3 at f_p $=0.002$, 0.03, and 0.07 for $n_p=1.5+i1.0$. Figures 8 and 9 (with Tables 5 and 6, respectively) are analogous to Figs. 6 and 7 (Tables 3 and 4) but with the refraction of the particles being equal to $n_p=2.8+i1.0$.

The first significant observation that can be made from inspection of this series of figures is the strong influence of electromagnetic couplings on the absorption and the scattering properties of the different ensembles of particles. Also, in the presence of absorption, both the total configuration average scattering and absorption cross sections, $\langle C_{sca}\rangle$ and $\langle C_{abs}\rangle$, decrease when the filling fraction is increased even for particles with $n_p=1.5$. These effects confirm experimental observations that while dependent scattering makes it difficult to perform particle size

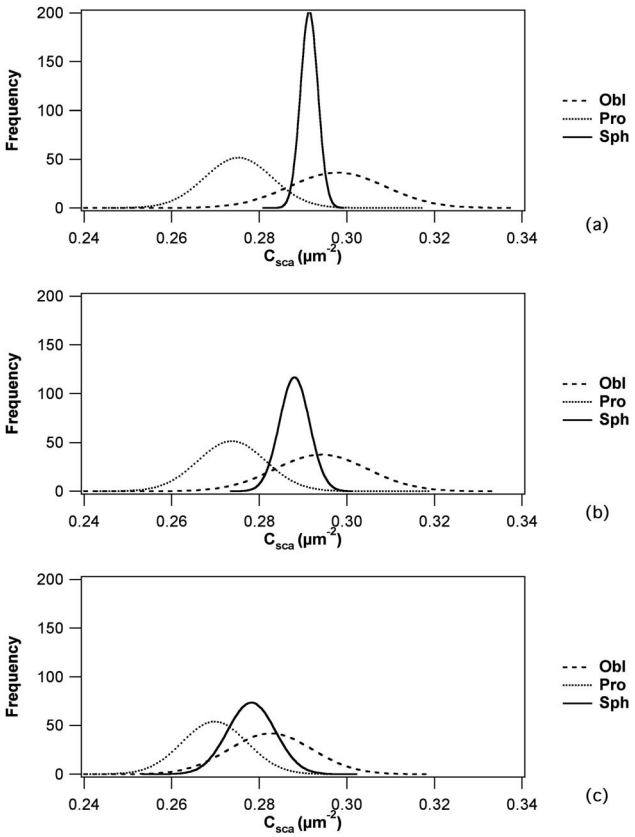

Fig. 6. Frequency as function of the scattering cross sections for the spherical, oblate, and prolate systems with index of refraction $n_p=1.5+i1.0$: (a) $f_p=0.002$, (b) $f_p=0.03$, (c) $f_p=0.07$.

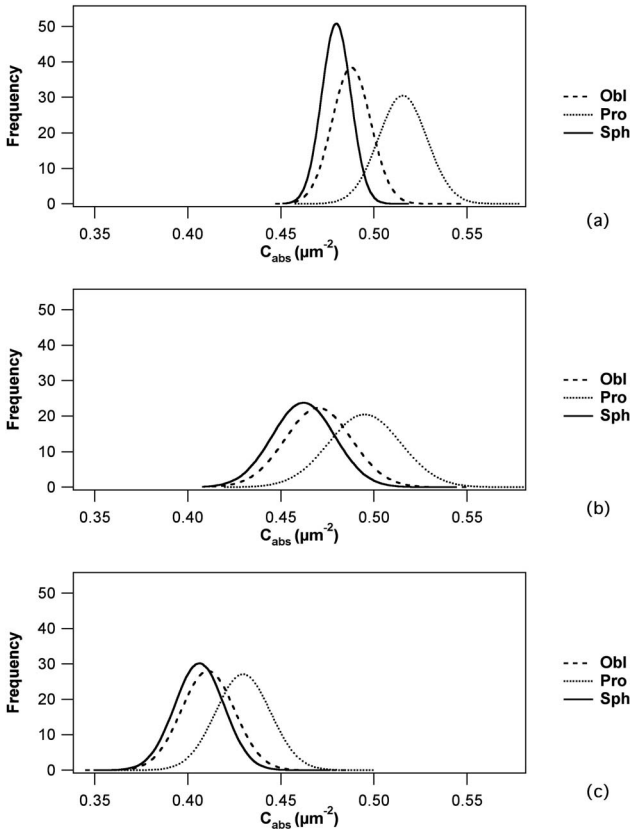

Fig. 7. Frequency as function of the absorption cross sections for the spherical, oblate, and prolate systems with index of refraction $n_p=1.5+i1.0$: (a) $f_p=0.002$, (b) $f_p=0.03$, (c) $f_p=0.07$.

analysis of dense colloidal systems, dependent absorption increases the complexity of predicting the color of a system via traditional color-matching analysis.

Another striking observation is the large difference occurring between the scattering properties of the systems composed of nonspherical with those composed of only spherical particles. At the lowest filling fraction (f_p $=0.002$) and for $n_p=2.8$, the standard deviation σ of the configuration average scattering cross sections $\langle C_{sca}\rangle$ of the ensemble of spheres is ten times smaller than the one calculated from the spheroids. For the highest concentration ($f_p=0.07$) it is still two times smaller. Tables 7 and 8 contain the independent orientation and polarization averaged absorption and scattering cross sections for the three systems. It shows differences in $\langle C_{abs}\rangle$ and $\langle C_{sca}\rangle$ ranging from 4% to 10% between the multiple sphere systems and those composed of spheroids, whereas the values of the corresponding single-particle albedos remain practically constant (around 0.48 and 0.36 for particles with $n_p=2.8$ and $n_p=1.5$, respectively). Thereby, one can conclude that in presence of absorption yielding a relatively large single-particle albedo, electromagnetic couplings amplify the influence of the shape on the possible modification of the scattering properties.

Finally, it can be observed that in some cases, the standard deviations of the scattering and absorption cross sections diminish when the concentration increases from f_p $=0.03$ to $f_p=0.07$. The origin of this phenomenon can be explained as follows: due to the noninterpenetrability of the heterogeneities, the probability to generate different

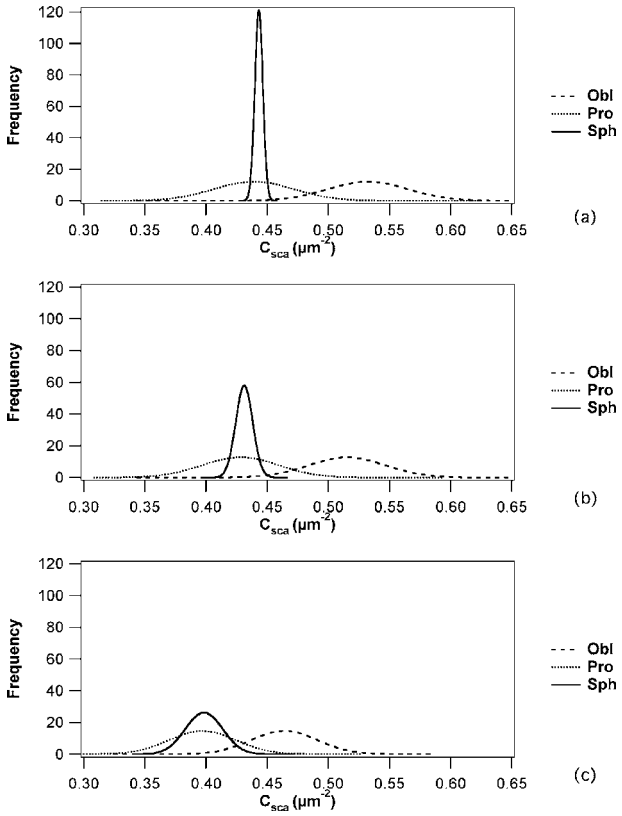

Fig. 8. Frequency as function of the scattering cross sections for the spherical, oblate, and prolate systems with index of refraction $n_p = 2.8 + i1.0$: (a) $f_p = 0.002$, (b) $f_p = 0.03$, (c) $f_p = 0.07$.

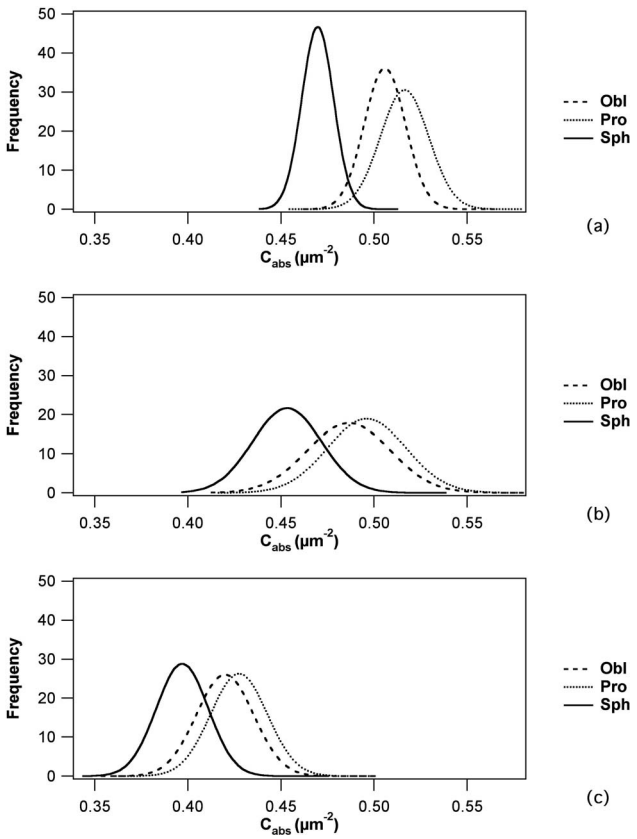

Fig. 9. Frequency as function of the absorption cross-sections for the spherical, oblate and prolate systems with index of refraction $n_p = 2.8 + i1.0$: (a) $f_p = 0.002$, (b) $f_p = 0.03$, (c) $f_p = 0.07$.

spatial configurations decreases as the filling fraction of the medium increases. Thus starting from a given concentration the probability to obtain a different value of the absorption or scattering cross sections from one configuration also diminishes, leading to a decrease in the corresponding standard deviations. For example, in the hypothetical case of close-packed identical spherical dielectric objects, there is only one possible configuration and the standard deviation vanishes.

5. CONCLUSION

We have presented a statistical method, which combined with the multiple T-matrix formalism allows the calculation of the configuration average scattering and absorption cross sections of ensembles of nonspherical particles with multiple-scattering interactions. We applied this methodology to study and compare the variations of the optical properties of three systems whose primary particles have the same volumes and same index of refraction but with different shapes. By varying the relative filling fraction of the systems, we were able to show the occurrence of dependent scattering and dependent absorption phenomena whose amplitudes are strongly influenced by the shape of the primary particles. The study was performed on a relatively small number of particles and at a

Table 7. Values of the Average Extinction Cross Sections Assuming Independent Scatterers for the Three Systems Having $n_p = 1.5$ and $n_p = 2.8$

n_p	1.5			2.8		
Shape	Oblate	Prolate	Sphere	Oblate	Prolate	Sphere
$\langle C_{ext} \rangle$	0.198	0.192	0.195	1.257	1.061	1.125

Table 8. Values of the Average Scattering and Absorption Cross Sections Assuming Independent Scatterers for the Three Systems Having $n_p = 1.5$ and $n_p = 2.8$

n_p	1.5+i1.0			2.8+i1.0		
Shape	Oblate	Prolate	Sphere	Oblate	Prolate	Sphere
$\langle C_{abs} \rangle$	0.502	0.505	0.484	0.515	0.513	0.473
$\langle C_{sca} \rangle$	0.283	0.285	0.292	0.489	0.487	0.446

single wavelength using an ordinary desktop computer. However, with adequate computing power, it could be easily extended to larger systems of scatters and to a wider spectrum of wavelengths. Also, the optical properties of an ensemble of particles are strongly linked to the size of the primary scatterers with respect to the wavelength of the incident radiation. Thereby the relative variations in the scattering and absorbing cross sections found in this work do not necessarily hold for larger or smaller particles.

Finally, this type of study does not allow one to bridge the fundamental gap between the microscopic and macroscopic optical characteristics of heterogeneous media. The calculations of this work provide information on only the scattering and absorption properties of an ensemble of particles dispersed in an infinite-surrounding medium. It is clear that in real systems boundary conditions should be taken into account. Furthermore, the excitation field on each particle should take into account the contributions of all the dispersed scatterers present throughout a macroscopic medium. Nevertheless, since the variations in the macroscopic properties are strongly linked to changes of the microscopic characteristics, we strongly believe that this method can be a useful tool of research in different fields of applied physics where optical properties of colloids are determinant factors. Notably, it can help in understanding the relations between variations of the intrinsic and extrinsic properties of the dispersed phase, such as size, shape, nature, and spatial distribution, and the change in scattering and absorption properties of the entire medium.

ACKNOWLEDGMENTS

The authors thank E. Nahmad (CIP Grupo Comex) for supporting the start-up of this work and Richard K. Chang for allowing its continuation and conclusion.

REFERENCES

1. B. T. Draine, "The discrete-dipole approximation and its application to interstellar graphite grains," Astrophys. J. **333**, 848–872 (1988).
2. K. S. Kunz and R. J. Luebbers, *Finite Difference Time Domain Method for Electromagnetics* (CRC Press, 1993).
3. P. C. Waterman, "Symmetry, unitary and geometry in electromagnetic scattering," Phys. Rev. D **3**, 825–839 (1971).
4. M. I. Mishchenko, "Light scattering by randomly oriented axially symmetric particles," J. Opt. Soc. Am. A **8**, 871–882 (1991).
5. F. M. Kahnert, J. J. Stamnes, and K. Stamnes, "Application of the extended boundary condition method to homogeneous particles with point group symmetries," Appl. Opt. **40**, 3110–3123 (2001).
6. M. I. Mishchenko, L. D. Travis, and A. A. Lacis, *Scattering, Absorption and Emission of Light by Small Particles* (Cambridge U. Press, 2002).
7. D. J. Wielaard, M. I. Mishchenko, A. Macke, and B. E. Carlson, "Improved *T*-matrix computations for large, nonabsorbing and weakly absorbing nonspherical particles and comparison with geometrical-optics approximation," Appl. Opt. **36**, 4305–4313 (1997).
8. T. Wriedt, "Using the *T*-Matrix method for light scattering computations by non-axisymmetric particles: superellipspoids and realistically shaped particles," Part. Part. Syst. Charact. **19**, 256–268 (2002).
9. F. M. Schulz, K. Stamnes, and J. J. Stamnes, "Scattering of electromagnetic waves by spheroidal particles: a novel approach exploiting the *T*-Matrix computed in spheroidal coordinates," Appl. Opt. **37**, 7875–7896 (1998).
10. D. W. Mackowski and M. I. Mishchenko, "Calculation of the *T* matrix and the scattering matrix for ensembles of spheres," J. Opt. Soc. Am. A **13**, 2266–2278 (1996).
11. E. Zubkoa, Y. Shkuratova, M. Hart, J. Eversole, and G. Videen, "Backscattering and negative polarization of agglomerate particles," Opt. Lett. **28**, 1504–1506 (2003).
12. J. Joshi, H. S. Shah, and R. V. Mehta, "Application of multiflux theory based on scattering by nonspherical particles to the problem of modeling optical characteristics of pigmented paint film: part II," Color Res. Appl. **28**, 308–316 (2003).
13. W. C. Chew, *Waves and Field in Inhomogeneous Media*, IEEE Press Series on Electromagnetic Waves (IEEE, 1990).
14. L. Tsang, J. A. Kong, and R. T. Shin, *Theory of Microwave Remote Sensing* (Wiley, 1985).
15. O. R. Cruzan, "Translation addition theorems for spherical vector wave functions," Q. Appl. Math. **20**, 33–40 (1962).
16. B. Stout, J.-C. Auger, and J. Lafait, "A transfer matrix approach to local field calculations in multiple-scattering problems," J. Mod. Opt. **49**, 2129–2152 (2002).
17. A.-K. Hamid, "Electromagnetic scattering by an arbitrary configuration of dielectric spheres," Can. J. Phys. **68**, 1419–1428 (1990).
18. K. A. Fuller, "Consummate solution to the problem of classical electromagnetic scattering by an ensemble of spheres. I: Linear chains," Opt. Lett. **13**, 90–92 (1988).
19. J.-C. Auger and B. Stout, "A recursive *T*-matrix algorithm to solve the multiple scattering equation: numerical validation," J. Acoust. Soc. Am. **79–80**, 533–547, (2003).
20. D. Mackowski, "Calculation of total cross sections of multiple-sphere clusters," J. Opt. Soc. Am. A **11**, 2851–2861 (1994).
21. B. Stout, J. C. Auger, and J. Lafait, "Individual and aggregate scattering matrices and cross sections: conservation laws and reciprocity," J. Mod. Opt. **48**, 2105–2128 (2001).
22. R. T. Wang, J. M. Greenberg, and D. W. Schuerman, "Experimental results of dependent light scattering by two spheres," Opt. Lett. **11**, 543–548 (1981).
23. J.-C. Auger, V. Martinez, and B. Stout, "Scattering efficiency of aggregated clusters of spheres: dependence on configuration and composition" J. Opt. Soc. Am. A **22**, 2700–2708 (2005).